Journal of the National Academy of Forensic Engineers®

http://www.nafe.org
ISSN: 2379-3252

Vol. XXXI No. 2 December 2014

Forensic Engineering Usage of Surveillance Video in Accident Reconstruction

By Richard M. Ziernicki, Ph.D., P.E. (NAFE 308F),
William H. Pierce, P.E. (NAFE 846C), and
Angelos G. Leiloglou, M. Arch.

Abstract

With the increased use of surveillance cameras, more and more video footage depicting accidents is available these days for accident reconstruction. The authors present an accident reconstruction case study involving an impact between a tractor-tanker and a pedestrian using surveillance video footage from a nearby business. Overall, the video footage is of poor quality, which is typical of surveillance video. This is usually evidenced by low frame rate, low resolution, and significant lens distortion — not to mention the fact that the video is not centered on the actual accident. This paper addresses a solution to minimize the error often associated with such surveillance video.

First, the distortion in the video footage is corrected using software that warps the image with a reverse distortion. Once the distortion in the video footage is corrected, then accurate photo/videogrammetry is performed to attain desired measurements. These measurements are then processed to perform a more accurate and detailed time/space analysis. Finally, graphics and photo-realistic animation are used to present the accident in time-space domain.

Keywords

Accident reconstruction, forensic engineering, video, pedestrian, animation, photogrammetry, barrel lens distortion, surveillance video, focal length

Introduction

The lead author of this paper was retained by the law firm representing the injured party in an accident that occurred between a pedestrian and tractor-tanker. The accident occurred in Florida at an intersection between Street A and Street B (**Figure 1**). The tractor-tanker was driving eastbound on Street A and stopped at

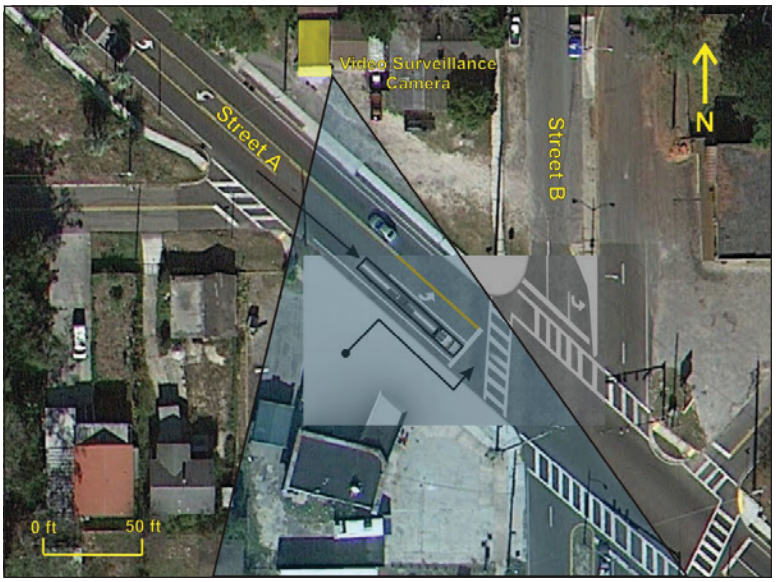

Figure 1
Aerial view of intersection (courtesy of Google Maps) showing eastbound tractor-tanker stopped at red light, pedestrian path, and video surveillance camera position.

Richard Ziernicki, P.E., 7185 South Tucson Way, Englewood, CO 80112-3987; (303) 925-1900; rziernicki@knottlab.com

a red light at the intersection of Street A and Street B. After the tractor-tanker stopped, the pedestrian began crossing the intersection in front of the tractor-tanker. While the pedestrian was crossing, the traffic signal for the tractor-tanker turned green, and the rig accelerated forward. The pedestrian was subsequently struck by the left side of the tractor-tanker's front bumper and knocked down, ultimately leading to the tractor's left-front tire running over the pedestrian's left leg. The tractor then came to a stop with the pedestrian lying directly in front of the tractor's second-axle left tire.

Across the street, a nearby business had a surveillance camera installed that happened to capture the accident (**Figure 2**). The video footage from this surveillance camera was used to perform a time-space analysis of both the pedestrian and the tractor-tanker.

Figure 2
Exterior surveillance camera of nearby business.

Surveillance Video Footage Correction and Enhancement

The overall quality of the raw surveillance video footage was very poor (**Figure 3**). As it was — with a frame size of only 352x240 pixels, a frame rate of 7.5 frames per second, and significant barrel lens distortion — the footage had to be corrected and enhanced before it could be used for any photogrammetric processing and engineering analysis.

Figure 3
Frame from raw surveillance footage.

The most adverse (unfavorable) problem with the surveillance video footage was the barrel lens distortion, which is attributed to the imperfections due to the physical characteristics of the camera lens and is commonly associated with wide-angle lenses like the one used by the surveillance camera. Barrel distortion, a type of radial distortion, is a quadratic function that increases as the square of the distance from the lens

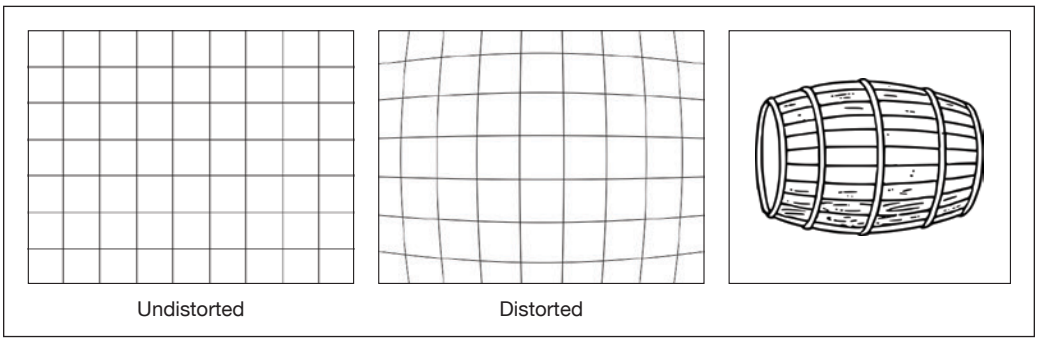

Figure 4
Barrel lens distortion.

center increases. The effect causes the image magnification to decrease as the distance from the center increases, causing straight lines to appear curved or bowed out toward the edges of the image like a barrel (**Figure 4**).

In order to use photogrammetry techniques to accurately attain measurements from the video frames, the lens distortion needed to be corrected. Many software applications (i.e., Photoshop, Premiere, PTLens, DxO Optics Pro, Syntheyes, Virtualdub) can correct for lens distortion automatically if the camera and lens used to capture the video is known. Because the camera used to record the accident in this case was not known, a manual method for lens distortion correction was applied.

The method used to correct the barrel lens distortion in the surveillance is based on the principle that straight lines in the real world would appear straight when viewed through a perfect lens. The road on which this accident occurred was straight and level. Therefore, the engineer was able to use the striping and curb lines seen in the surveillance video as a guide to determine how much the image needed to be "un-distorted" to correct for the barrel distortion using the custom parameters of the lens correction filter in Adobe Photoshop (**Figure 5**). This correction was then applied to all the frames in the video surveillance footage.

Figure 5
Surveillance video with lens distortion (left). Surveillance video corrected to eliminate barrel lens distortion (right).

Once the lens distortion was corrected, the footage was further enhanced by adjusting the levels of tonal range/color balance and sharpening the edges to improve the clarity of the subject vehicles and important landmarks in the video.

Solving the Camera

Finally, the position, orientation, and focal length of the camera were solved using the inverse camera method in Photomodeler, a software package based on the science of photogrammetry. The virtual 3D camera solved in the previous step, along with the control points of the accident scene, were then imported into a 3D animation package and matched to the corrected/enhanced surveillance video.

Tractor-Tanker Position and Velocity Versus Time Using Video Footage

Using measurements obtained during inspection of the tractor-tanker, a scaled 3D model of the tractor-tanker was created in Maya, a modeling and animation software product developed by Autodesk

(**Figure 6**). The modeled tractor-tanker was then placed in the virtual accident scene. For each surveillance video frame, the modeled tractor-tanker was aligned with the actual tractor-tanker seen in the video (**Figure 7**), and the position of the modeled tractor-tanker was recorded.

Figure 6
3D computer-generated model of tractor-tanker.

After establishing the tractor-tanker's position data for each of the frames, the position data was used to determine the instantaneous velocity between each of the position points (**Figure 8**). The instantaneous tractor-tanker's velocity determined from position data at 7.5 frames per second varied erratically. The variance in instantaneous velocity was attributed to the sensitivity in the determined tractor-tanker's positions between each frame spaced only 0.13 seconds apart. For example, 4 inches of position error between two adjacent frames would result in an instantaneous velocity error of 2.5 feet per second (fps). Therefore, the instantaneous tractor-tanker's velocity was determined to not be very helpful for forensic engineering purposes.

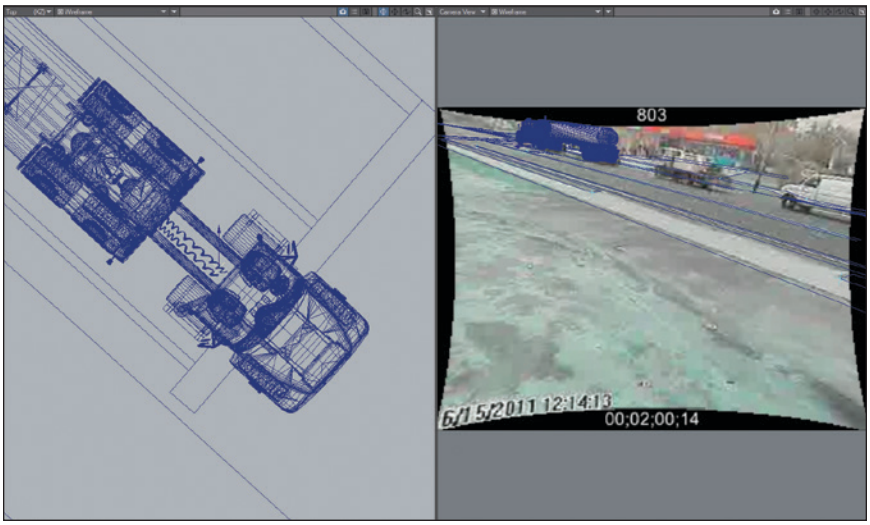

Figure 7
Virtual tractor-tanker aligned with tractor-tanker depicted in video.

In order to smooth the velocity data, an iterative process was performed to separate groups of points from within the plotted tractor-tanker position versus time data that could be assigned good-fit 1st and 2nd order polynomials. The second derivative of each polynomial was calculated

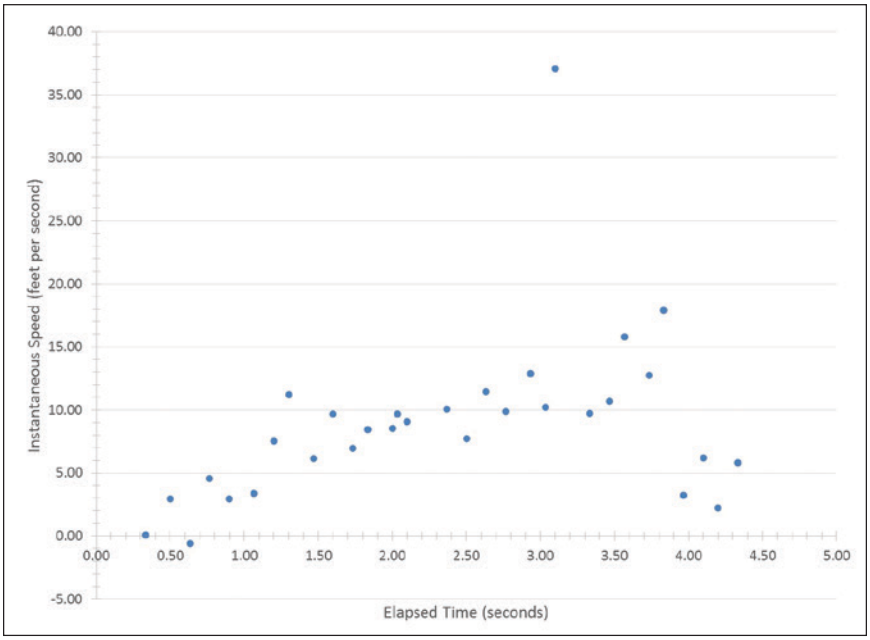

Figure 8
Instantaneous tractor-tanker velocity versus time from position data at 7.5 fps.

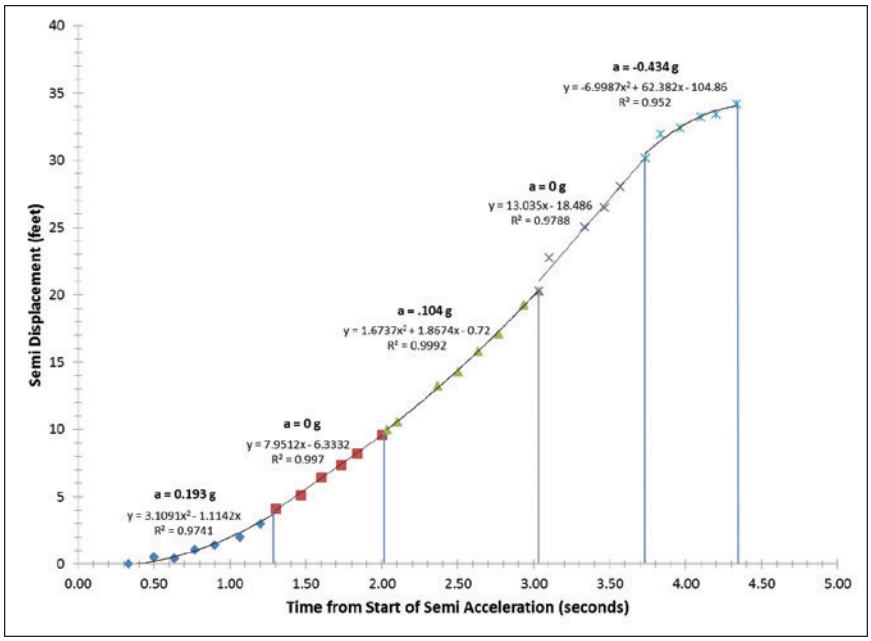

Figure 9
Plotted tractor-tanker position data with 1st and 2nd order polynomials and calculated acceleration.

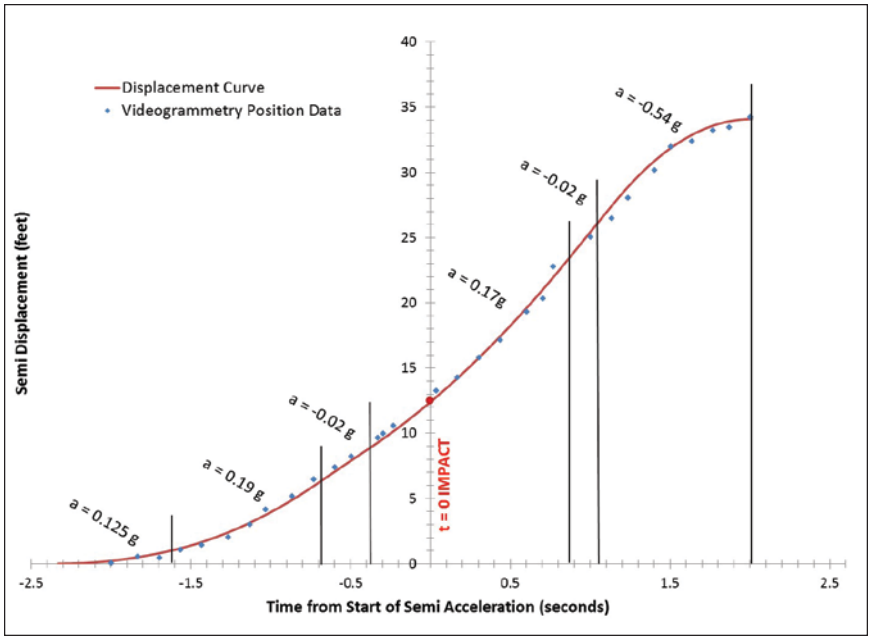

Figure 10
Plotted tractor-tanker position data with best-fit curve.

to determine the tractor-tanker's approximate acceleration versus time (**Figure 9**).

The approximate acceleration values were then integrated from the polynomials in 0.02 second time-steps to determine position as a function of time. An iterative process was performed by adjusting the acceleration values until the resulting position versus time curve best matched the position versus time data points obtained from the videogrammetry process (**Figure 10**). Once the acceleration values were determined, the acceleration values were integrated to determine velocity as a function of time (**Figure 11**).

Tractor-Tanker Engine Speed Versus Time

After determining the position, velocity, and acceleration of the tractor-tanker as a function of time, the tractor-tanker's engine speed was calculated as a function of time. First, published gear ratios and the tractor-tanker's tire size were used to determine the engine speed as a function of velocity. The tractor's tachometer redline occurs at an engine speed of 2,200 rpm. In first gear, 2,200 rpm occurs at a speed of 13.3 fps.

However, the tractor got up to a speed of approximately 15 fps. Therefore, there was a likely transition into second gear at some point prior to reaching that speed. Based on the tractor-tanker's velocity versus time chart, there was only one brief period of time before the tractor-tanker reached 15 fps in which a very gentle deceleration occurred. This period corresponded to the timing of a typical gear shift. Therefore,

it was determined the gear shift occurred in the short period of deceleration. The calculated engine speed was plotted as a function of time (**Figure 12**).

Pedestrian Seen in Surveillance Video

After determining the tractor-tanker's position, velocity, and engine speed as a function of time, the pedestrian's movement leading to impact was reconstructed using the video surveillance footage.

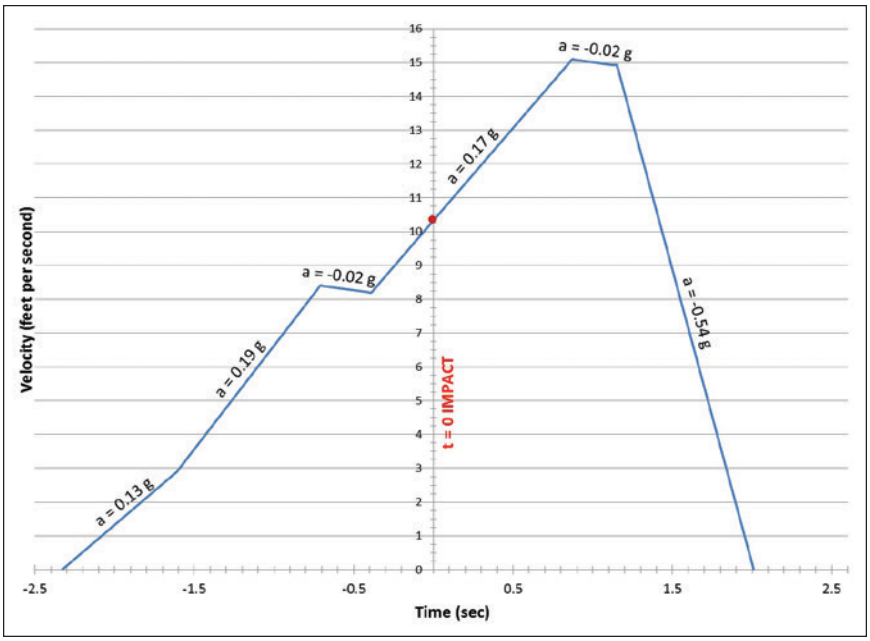

Figure 11
Plotted tractor-tanker velocity versus time.

The pedestrian is first seen in the surveillance video walking toward the sidewalk from a convenience store. The pedestrian stopped walking near point P0, as shown in **Figure 13**. As the pedestrian was stopped at point P0, the tractor-tanker came to a stop at the intersection, obstructing the view of the pedestrian from the surveillance camera. After the tractor-tanker had stopped, the pedestrian appeared in the surveillance video frames from under the tanker walking from point P1 to point P2. After point P2, the pedestrian was obstructed from view due to the semi-tractor's position between the pedestrian and camera. Shortly after the tractor-tanker started moving, the pedestrian came briefly into frame again at point P5 from under the front of the tractor. The pedestrian came into frame again at impact point P7.

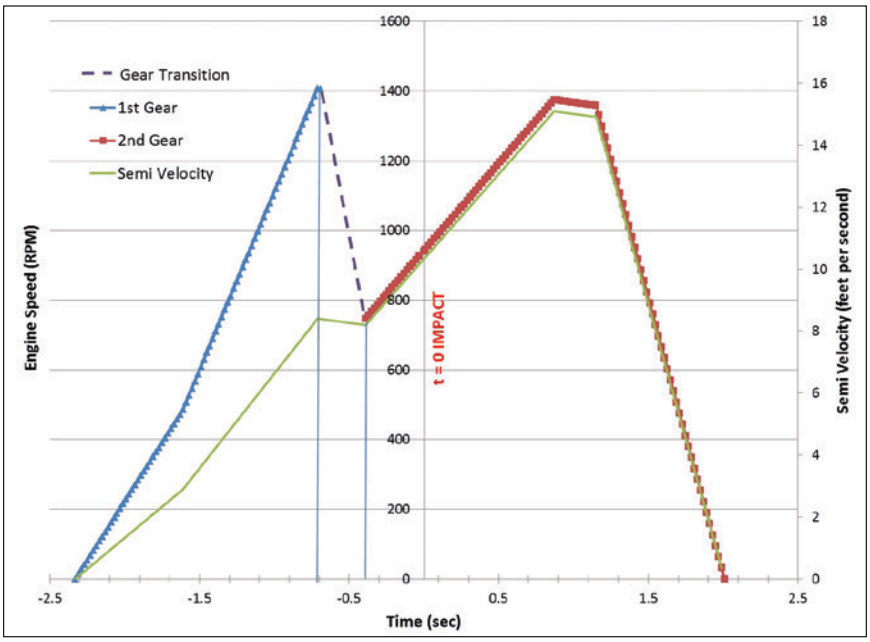

Figure 12
Tractor-tanker engine speed versus time.

Pedestrian Position and Velocity Versus Time

The methods that were used to determine the tractor-tanker's time-space could not be applied to determine the pedestrian's time-space because the pedestrian appeared very small and pixelated in the video,

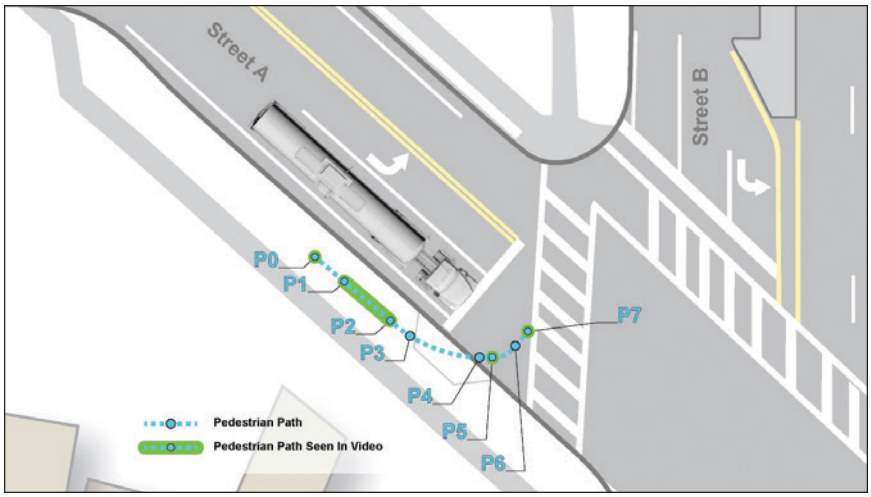

Figure 13
Path of pedestrian to impact.

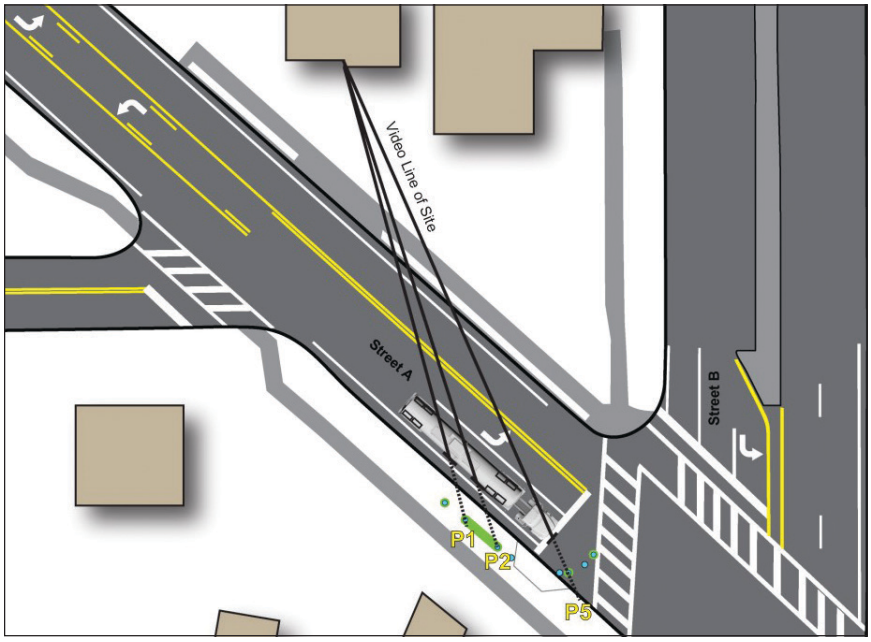

Figure 14
Line-of-site method used to determine range of positions for points P1, P2, and P5.

and the pedestrian was obstructed from view in many frames. The tractor-tanker time-space analysis, video camera's line-of-site, and published pedestrian walking speed data were used to determine the pedestrian's time-space during the accident sequence.

The pedestrian's position at the point of impact (P7) was first analyzed. The pedestrian was visible on the surveillance video as she was struck by the left front bumper of the semi-tractor. The known position of the semi-tractor at the point of impact and the impact point on the tractor's left front bumper were used to precisely locate the pedestrian at the point of impact (P7).

After determining the pedestrian's position at the point of impact, attention was directed at the points in the video sequence where the pedestrian could be seen, such as under the semi-tanker walking between points P1 and P2. The pedestrian could also be briefly seen in the surveillance video from under the front of the semi-tractor at point P5. The video line-of-site method was used to determine the range of positions at points P1, P2, and P5. The range of possible pedestrian positions is depicted as dotted lines in **Figure 14**.

Two constraints and a reasonable assumption were applied in order to determine pedestrian positions P1 and P2. One constraint was that positions P1 and P2 fell along the camera's line-of-site shown in **Figure 14**. A second constraint was that positions P1 and P2 were between the tanker and a vehicle that had been parked partially on the sidewalk. The applied assumption was the pedestrian walked in a straight path that was parallel with the direction of the sidewalk. With the given constraints and assumption,

P1 and P2 were chosen such that the distance between the points (when divided by the known time between points P1 and P2) best matched the 50th percentile walking velocity of a 40-year-old woman pedestrian (5.3 fps). The fastest velocity that could be obtained with the constraints and assumption was 3.79 fps. Therefore, the path corresponding to the fastest velocity of 3.79 fps was chosen.

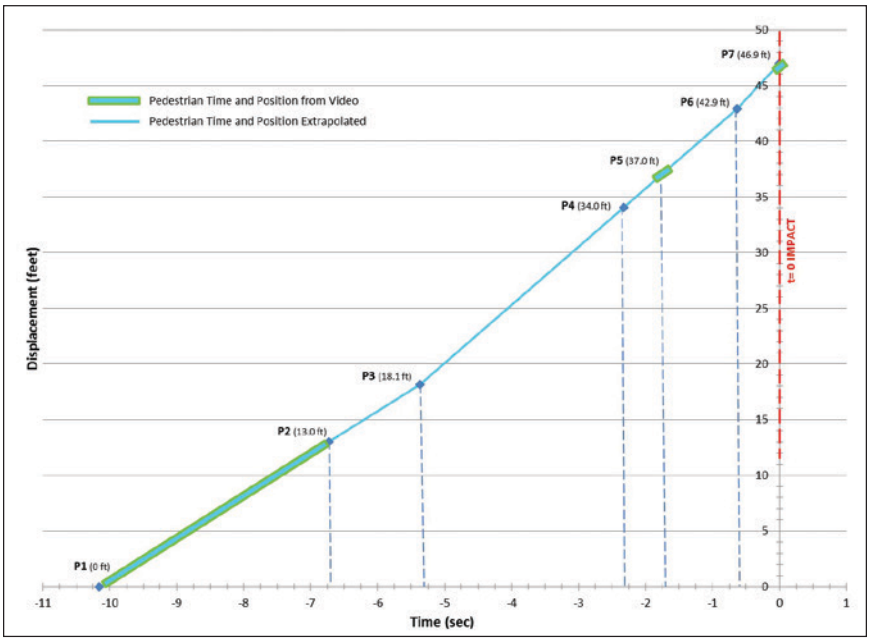

Figure 15
Pedestrian's position versus time.

After determining the pedestrian positions at points P1 and P2, the position of the pedestrian at point P6 was determined. Point P6 corresponds to the point in time the pedestrian testified that she heard the tractor's gears and began to walk fast. The authors of this paper assumed that she heard the gears at the time the tractor likely switched from first to second gear. The gear transition was previously determined to occur 0.63 seconds prior to impact. In order to determine the position at point P6, it was estimated the pedestrian walked along the quickest path to get out of the way of the semi-tractor, according to the 85th percentile walking velocity for a 40-year-old woman pedestrian (6.4 fps). The resulting distance between points P6 and P7 was 4 feet.

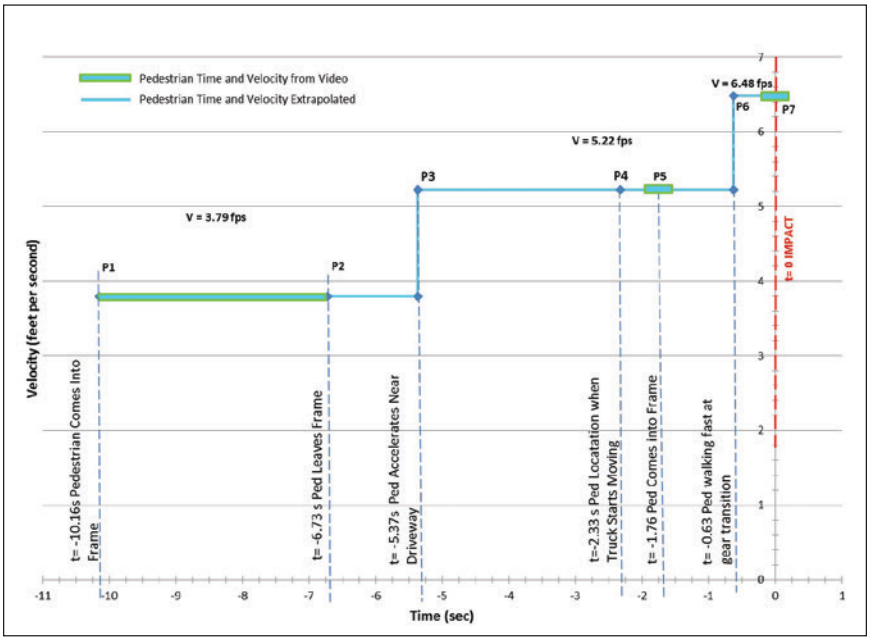

Figure 16
Pedestrian's velocity versus time.

Next, the position of the pedestrian at point P5, corresponding to the location the pedestrian came into video frame from under the semi-tractor, was determined. The timing at point P5 was known as well as the range of possible positions based on the surveillance camera's line-of-site (**Figure 14**). A series of iterations was performed, changing the pedestrian position P5 until the distance between points P5 and P6

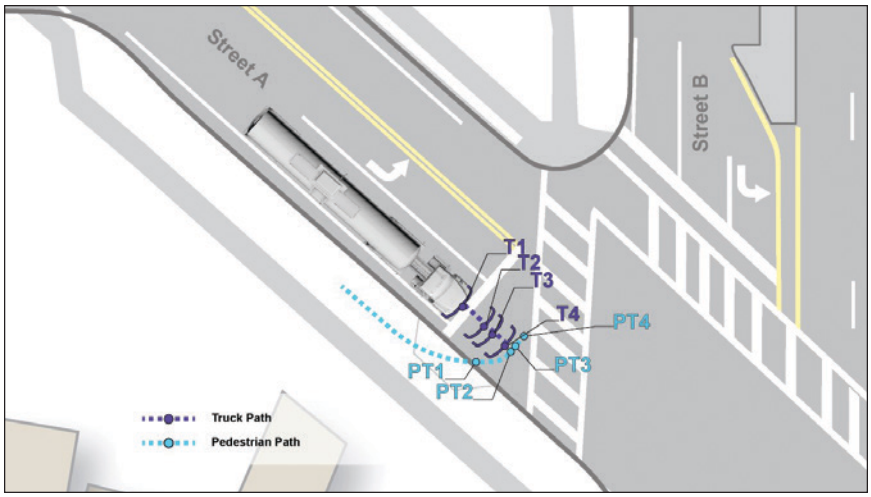

Figure 17
Tractor-tanker and pedestrian time-space diagram.

Figure 18
Still frame taken from photo-realistic animation.

(when combined with the timing between points P5 and P6) best matched the pedestrian's initial velocity of 3.79 fps. The minimum velocity that could be obtained between points P5 and P6 was 5.22 fps, which is near the 50th percentile walking velocity for a 40-year-old woman pedestrian.

Next, it was estimated that the pedestrian continued to travel in a straight path parallel to the sidewalk at a constant speed after point P2 until she started turning at point P3. The turning position (P3) was chosen at the edge of a driveway because the driveway slopes downward toward the road, providing a convenient location to walk down to street level.

After determining turning point P3, the path between points P3 and P5 was determined. In order to determine the path between points P3 and P5, the lowest possible velocity between points P3 and P5 was calculated based on a straight path between P3 and P5. The lowest velocity was determined to be 5.12 fps, which is near the pedestrian's velocity between points P5 and P6 of 5.22 fps. The forensic engineer assumed that the pedestrian traveled at a constant velocity after turning at the driveway. An arched path was chosen such that the distance and timing between points P3 and P6 corresponded to a constant 5.22 fps. After the position and velocities of the pedestrian were determined, time-space diagrams were prepared as shown in **Figure 15** and **Figure 16**.

Combining Tractor-Tanker and Pedestrian in a Time-Space Diagram

After determining the time-space of the tractor-tanker and the pedestrian, a combined pedestrian and tractor-tanker time-space diagram was prepared (**Figure 17**) as well as photo-realistic animations created in Autodesk Maya (**Figure 18**).

Conclusion

Video surveillance cameras occasionally capture and record accidents. Despite significant camera lens distortion, low frame rate, and low resolution frequently encountered with surveillance video, forensic engineers can apply several methods to perform high-quality accident reconstructions from the surveillance video footage.

The authors first corrected the lens distortion using software packages such as Adobe Premiere and Photoshop. PhotoModeler was then used to accurately locate the position, orientation, and focal length of the camera in virtual space. By placing the virtual vehicle model(s) in the virtual space, the position of the vehicle(s) in each video frame was determined. This process is a function of photogrammetry. By using methods addressed in this paper, smoothed position and velocity versus time curves were created from the raw position data captured at approximately 0.133 of a second time increment. Furthermore, engine rpms, gear shifting, as well as impact speed of vehicle(s), were obtained using the surveillance video and published engine specifications.

The authors also used a method to reconstruct the motion of smaller objects seen in surveillance video, such as pedestrians, which often appear very small and highly pixelated. However, the camera's line-of-site method described in this paper can be used to constrain the range of possible pedestrian positions for each video frame. Published walking speed data can be used to estimate the pedestrian positioning in each video frame.

In summary, the video surveillance footage, even at very poor quality, can be used effectively by forensic engineers with the application of proper scientific methods. Those methods are a strong basis for foundation of the accident reconstruction and are considered by courts in the process of qualification of a forensic engineer as an expert in a court of law.

Bibliography

T. Thomahlen, H Broszio, and Ingold Wassermann. "Robust Line-Based Calibration of Lens Distortion from a Single View," in *Proceedings of Mirage 2003 (Computer Vision/Computer Graphics Collaboration for Model-based Imaging, Rendering, Image Analysis and Graphical Special Effects*, pp. 105-112. Rocquencourt, France, 2003.

W. Kim, C. Kim. "An Efficient Correction Method of Wide-Angle Lens Distortion for Surveillance Systems," in *Proceeding of Circuits and Systems*, pp. 3206-3209. Taipei, Taiwan, May 24-27, 2009.

F. Devernay and O. Faugeras. "Straight Lines Have to be Straight: Automatic Calibration and Removal of Distortion from Scenes of Structured Environments." *Machine Vision and Applications*, vol. 13, no. 1, Pp. 14-24, August 2001.

W. Hugemann. "Correcting Lens Distortions in Digital Photographs." Copyright 2010 by EVU.

J. Eubanks, P. Hill. *Pedestrian Accident Reconstruction and Litigation*. Tucson, Arizona: Lawyers & Judges Publishing Co., Inc. 1999.

2003 Diesel Truck Index. Santa Ana, California: Truck Index, Inc. 2003.

Richard M. Ziernicki, David A. Danaher, Jeff Ball. "Forensic Engineering Evaluation of Physical Evidence in Accident Reconstruction", *Journal of the National Academy of Forensic Engineers*, December 2007.

Richard M. Ziernicki, David A. Danaher. "Forensic Engineering and the Use of Computer Animations and Graphics", *Journal of the National Academy of Forensic Engineers,* December 2006.

Stephen Fenton, Wendy Johnson, James LaRocque, Nathan Rose and Richard Ziernicki. "Using Photogrammetry to Determine Equivalent Barrier Speed", *Society of Automotive Engineers (SAE)* paper 1999-01-0439, 1999.